

# Less is More: Surgical Phase Recognition from Timestamp Supervision

Zixun Wang<sup>1</sup>, Xinpeng Ding<sup>1</sup>, Wei Zhao<sup>2</sup> and Xiaomeng Li<sup>1</sup>

<sup>1</sup>The Hong Kong University of Science and Technology

<sup>2</sup>Beihang University

craddywang@gmail.com, xdingaf@connect.ust.hk,  
zhaow20@buaa.edu.cn, eexmli@ust.hk

## Abstract

Surgical phase recognition is a fundamental task in computer-assisted surgery systems. Most existing works require expensive frame-wise annotations, which is very time-consuming. In this paper, we introduce timestamp supervision to surgical phase recognition for the first time, which only requires randomly labeling one frame for each phase in a video. With timestamp supervision, current methods in natural videos aim to generate pseudo labels of full frames. However, due to the surgical videos containing ambiguous boundaries, these methods would generate many noisy and inconsistent pseudo labels, leading to limited performance. We argue that less is more in surgical phase recognition, *i.e.*, less but discriminative pseudo labels outperform full but ambiguous frames. To this end, we propose a novel method called uncertainty-aware temporal diffusion to generate trustworthy pseudo labels. Our approach evaluates the confidence of generated pseudo labels based on uncertainty estimation. Then, we treat the annotated frames as anchors and make pseudo labels diffuse to both sides, starting from anchors and stopping at the high-uncertainty frames. In this way, our proposed method can generate contiguous confident pseudo labels while discarding the uncertain ones. Extensive experiments demonstrate that our method not only significantly save annotation cost, but also outperforms fully supervised methods. Moreover, our proposed approach can be used to clean noisy labels near boundaries and improve the performance of the current surgical phase recognition methods.

## 1 Introduction

Computer-assisted surgery systems can improve the surgery’s quality and ensure the patients’ safety in modern operating rooms [33]. Surgical phase recognition is one key component of computer-assisted surgery systems, which

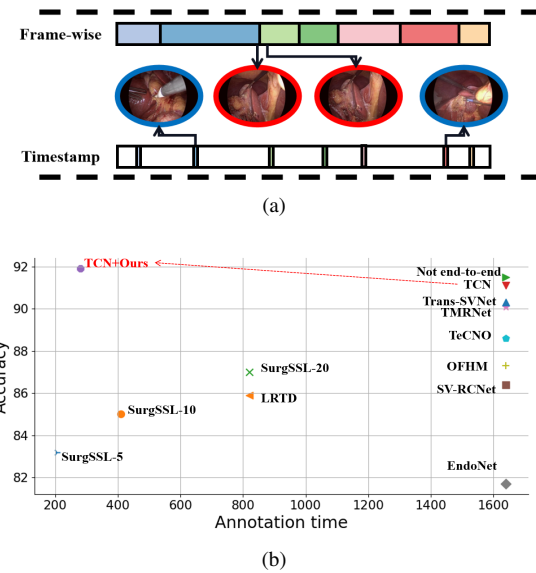
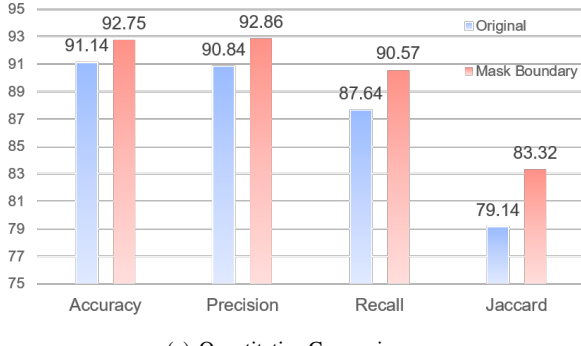
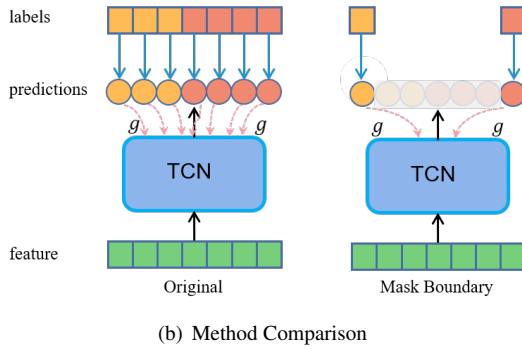


Figure 1: (a) Frame-wise annotations vs timestamp annotations. (b) Compared with existing methods, our method achieves the best performance and significantly saves annotation time.

aims to predict which phase is occurring at the current frame [20, 22]. It can be used for automatic indexing of surgical video databases [46], monitoring surgical process [4], scheduling surgeons [1] and assessing surgeons’ skills [30]. In recent years, automated surgical phase recognition has featured deep learning [16, 31, 41] and has reached promising recognition performance [6, 13, 46]. Most current surgical phase recognition approaches require expensive frame-wise annotations from surgeons. Moreover, surgery usually involves a series of coherent actions, making it difficult for surgeons to provide accurate and consistent phase labels at boundaries [19]; see red circles in Fig. 1(a). However, most existing approaches ignored this issue and treated all the frame-wise annotations as trustworthy labels.



(a) Quantitative Comparison



(b) Method Comparison

Figure 2: (a) Quantitative and (b) Method Comparison between original phase recognition model and directly masking boundaries under fully-supervised setting, *i.e.*, with frame-wise annotations. The backbone for both models is TCN [29].

This paper introduces the first **timestamp supervision** to surgical phase recognition, which only requires **randomly labeling one frame for each phase in a video**; see Fig. 1(a). Compared to existing fully-supervised and label-efficient surgical phase recognition [22, 39, 40], timestamp supervision not only has the minimum annotation cost but also avoid training with ambiguous boundary labels. Fig. 1(b) shows that our method achieves the best performance and significantly saves annotation time.

With timestamp supervision, one naïve solution is to train the model only with annotated frames, which achieves limited performance; see results in Table. 2. Some researchers in the computer vision area proposed to detect the action changes between two consecutive labeled frames for action recognition in natural videos with timestamp supervision [29]. However, this method displays limited performance to surgical videos because surgical videos contain more ambiguous boundaries, leading to the noisy and inconsistent pseudo labels; see Sec. 4.4 for detailed discussion.

To this end, we introduce a novel **Less is More (LiM)** method to perform surgical phase recognition from timestamp supervision motivated by the following two reasons. First, actions in the surgical video are continuous, which

shows a desirable temporal property that the closer the frames to the annotated timestamp, the more likely they are to be classified to the same label as the annotated one. Frames far from the annotated timestamp are difficult to have correct pseudo labels. Second, based on the observation that directly masking some frames at boundaries from full supervision can immediately get a clear improvement; see results in Fig. 2. This is because the ground-truths, *i.e.*, the human annotations, are inconsistent for these ambiguous boundaries [19] and these noisy labels will mislead the model. Based on the above motivations, our method consists of two modules **Uncertainty-Aware Temporal Diffusion (UATD)** and **Loop Training (LP)**. In Uncertainty-aware Temporal Diffusion, we first treat the annotated frames as anchors, *i.e.*, the starting points of pseudo-labeling, and make pseudo labels diffuse to both sides starting from the anchors. Afterward, the diffusion would be stopped by the high-uncertainty frames near phase boundaries by setting a threshold because these frames are ambiguous to be classified to any phase. Finally, we train the models with generated pseudo labels in an iterative way, *i.e.*, what we called Loop training.

The main contributions of this work can be summarized as the following:

- To our best knowledge, this is the first work that studies surgical phase recognition with the most annotation-efficient setting, *i.e.*, timestamp supervision.
- By the observation of ambiguous frames near the boundaries, we find that *less is more*, *i.e.*, using less but discriminative pseudo labels, can achieve better performance than the full but noisy ones.
- We introduce a novel uncertainty-aware temporal diffusion to generate confident pseudo labels based on the timestamp supervision, which generates rich and clean pseudo labels.
- We evaluate that our proposed approach can be used to clean noisy labels near boundaries, and improve the performance of the current surgical phase recognition methods.
- Our model-agnostic method is simple yet effective. Extensive experiments on two public benchmarks reveal that our method not only outperforms baseline by a large margin but also achieves better performance than the fully supervised methods. Our code will be released at GitHub upon acceptance.

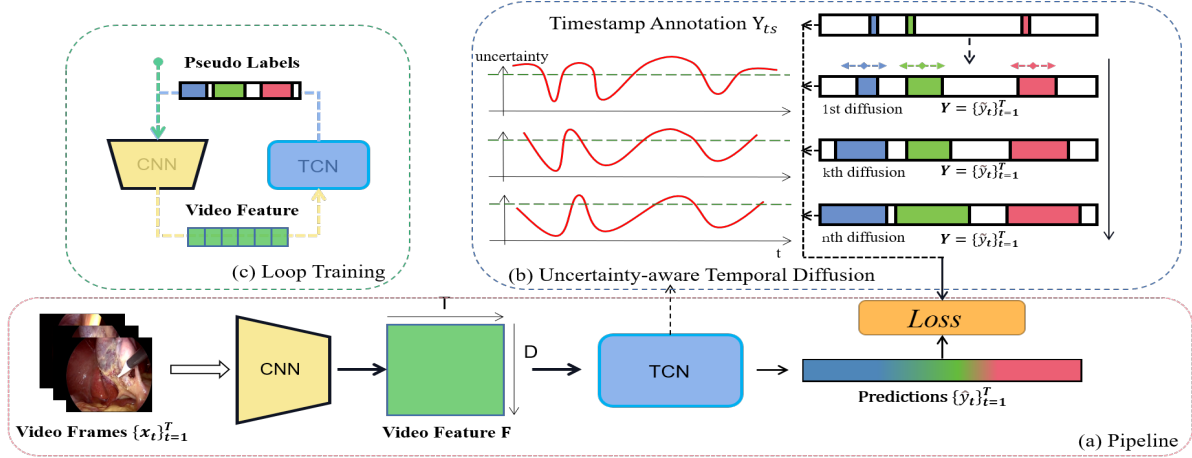


Figure 3: Overview of the training of our proposed method. (a) We feed the video frames into a CNN backbone following by a temporal convolutional network (TCN) to obtain the predictions. (b) We evaluate the uncertainty of predictions of each frame, based on which we make pseudo labels diffuse starting from annotated frames to both sides to generate the trustworthy labels. (c) Our model is trained in a loop manner, *i.e.*, the pseudo labels generated by TCN in current iteration is used to supervise the CNN in the next iteration.

## 2 Related Work

### 2.1 Surgical Phase Recognition

We broadly classified related methods for surgical phase recognition into two categories including fully-supervised learning and label-efficient learning.

**Fully-supervised Learning.** In fully-supervised learning, each frame in a surgical video is labeled. Early works [2, 15, 24] use hand-crafted features such as color and texture to perform recognition, which achieves limited performance and poor generalization. With the development of neural networks, recent deep learning based methods achieve the great success [6, 11, 13, 20–22, 46, 50, 51, 54]. EndoNet [46] first uses a convolutional neural network to automatically learn features and prove its effectiveness for surgical phase recognition. SV-RCNet [20] integrates CNN and LSTM to learn both spatial and temporal representations in an end-to-end way. To capture the long-range temporal relationship, TMRNet [22] introduces a memory bank and TeCNO [5] uses dilated temporal convolutional network to get a large receptive field. Recently, Yi *et al.* [50] realize the negative effect of hard frames and propose data cleansing and online hard frames mapper to detect and handle them respectively. Yi *et al.* [51] find that simply applying multi-stage architecture *e.g.* multi-stage TCN makes the refinement fall short and thus design not end-to-end training manner to alleviate this problem. Trans-SVNet [13] proposes a hybrid embedding aggregation Transformer to fuse spatial and temporal embedding. Ding *et al.* [6] emphasize the importance of segment-level semantics and extract semantic-consistent segments to refine the erroneous predictions. Notably, some related methods [5, 21, 46] utilize additional tool presence

labels to perform a multi-task learning to facilitate surgical phase recognition.

**Label-efficient Learning.** Despite the great success the above methods get, they require a large amount of annotated videos, which is very costly. To reduce the annotation cost, some researchers develop the data-efficient methods [9, 39, 40, 49, 52]. LRTD [39] introduces active learning to this context. It captures the long-range temporal dependency among continuous frames in the unlabeled data pool and selects the clips with weak dependencies to annotate. Other works [40, 49, 52] propose a video-level semi-supervised setting where only a portion of the video is annotated. Yengerer *et al.* [49] introduce self-supervised pre-training ensuring all available laparoscopic videos can be utilized. Yu *et al.* [52] propose a teacher/student approach where the teacher is trained on a small set of labeled videos and generates pseudo labels on the rest of unlabeled videos for student model learning. Furthermore, SurgSSL [40] uses consistency regularization and pseudo labeling to leverage the knowledge in unlabeled data, which progressively leverages the inherent knowledge held in the unlabeled data to a larger extent.

Compared with previous methods in surgical video analysis, our proposed timestamp supervision has **the minimal annotation cost**. According to annotation information provided in [32], the annotation efforts required in our method is one-sixth of that in a fully-supervised setting.

### 2.2 Weakly Supervision for Video Understanding

Weakly supervision has received widespread attention in some video understanding tasks, such as temporal action localization [7, 8, 36, 37, 42, 47] and action segmenta-

tion [3, 18, 25]. Some of them use video-level supervision, *i.e.*, a set of action categories, while some use transcript-level supervision, *i.e.*, an ordered list of actions. For example, Richard *et al.* [38] leverage text-based grammar from unordered action sets while Huang *et al.* [18] evaluate all possible alignments by given ordered actions. Although they significantly reduce the annotation effort, the performance is quite limited.

To trade-off the annotation-efficient and performance, timestamp supervision [29, 32, 34, 35] is proposed for action recognition. Specifically, Moltisanti *et al.* [35] propose a sampling distribution to select positive training frames around annotated frames. SF-Net [32] designs an action frame mining and a background frame mining strategy to introduce more negative frames into the training process. However, the above methods aiming at temporal action localization task generate very limited pseudo labels, is not suitable for surgical phase recognition, *i.e.*, frame-wise recognition. In the action segmentation task, to generate frame-wise pseudo labels, Li *et al.* [29] detect the action change between two consecutive timestamps by stamp-to-stamp energy function and generate full pseudo labels. However, in surgical videos, the frames near boundaries are generally ambiguous, the generated pseudo labels may be noisy annotations, which degrades the performance. Compared with previous approaches, our proposed method generates as many confident pseudo labels as possible by considering the temporal relationships among frames, while discarding pseudo labels with a large uncertainty.

### 3 Method

#### 3.1 Problem Definition and Pipeline

Let  $V = \{(x_t, y_t)\}_{t=1}^T$  be a video with  $T$  frames, where  $x_t$  is the  $t$ -th frame and  $y_t \in \{0, 1, \dots, C\}$  is the corresponding label with  $C$  class categories (0 denotes the unlabeled frames). Each surgical video is divided into several phases, and there is no overlapping among phases. Formally, we denote a phase as  $A_c = \{(x_t, y_t) \mid y_t = c\}_{t=s_c}^{e_c}$ , where  $s_{c+1} = e_c + 1$ .  $c$ ,  $s_c$  and  $e_c$  refer to the phase category, the start frame and the end frame of each phase, respectively. All phases construct a partition of  $V$  that  $\bigcup_c A_c = V$ ,  $\bigcap_c A_c = \emptyset$ . In timestamp supervision, each phase  $A_c$  has only singe timestamp label, *i.e.*,  $y_{t_c}$  ( $s_c \leq t_c \leq e_c$ ). That is to say,  $\sum_{t=s_c}^{e_c} \mathbb{1}(y_t \neq 0) = 1$  where  $\mathbb{1}(\cdot)$  is the indicator function. We denote this timestamp supervision as  $Y_{ts} = \{y_t \mid \sum_{t=1}^T \mathbb{1}(y_t \neq 0) = C\}$ .

To perform surgical phase recognition from timestamp supervision, we propose an uncertainty-aware temporal diffusion to generate the trustworthy pseudo labels in a loop manner, as shown in Fig. 3. We first feed video frames  $\{x_t\}_{t=1}^T$  into a CNN model  $f(\cdot)$ , *e.g.*, inception-v3 [43] in

our experiments, to extract the spatial features  $\mathbf{f}_t \in \mathbb{R}^D$  of each frame  $x_t$ , where  $D$  indicates the feature dimension. The features of each frame  $\mathbf{f}_t$  are aggregated to form a video feature  $\mathbf{F} = [\mathbf{f}_1 \ \mathbf{f}_2 \ \dots \ \mathbf{f}_T]^T \in \mathbb{R}^{T \times D}$ . Following is a temporal convolutional network (TCN)  $g(\cdot)$  [29] to capture the temporal relation of frames and generate the predictions for each frame, which can be denoted as  $\{\hat{y}_t\}_{t=1}^T$ , as shown in Fig. 3 (a). Then, we use the uncertainty estimation to evaluate the confidence of the predictions of each frame, which is denoted as  $u_t$ . After that, a temporal diffusion pseudo-labeling module is introduced to generates trustworthy pseudo labels  $\{\tilde{y}_t\}_{t=1}^T$  based on  $\{\hat{y}_t\}_{t=1}^T$  and  $\{u_t\}_{t=1}^T$ , as shown in Fig. 3 (b); see Sec. 3.2 for details. Finally, we use these generated pseudo labels to supervise the model in a loop manner, as shown in Fig. 3 (c); see Sec 3.3 for details.

#### 3.2 Uncertainty-aware Temporal Diffusion

To train the model with the timestamp supervision  $Y_{ts}$ , we need to generate more pseudo labels to obtain a discriminative model. In addition, frames in boundaries show very similar appearance [19], the generated pseudo labels boundaries may be ambiguous, which degrades the performance; see Fig. 2 for details.

Hence, we propose an uncertainty-aware temporal diffusion (UATD), which not only generates sufficient pseudo labels but also avoids noisy labeling. To this end, we first introduce an uncertainty estimation using Monte Carlo Dropout [12] to evaluate the confidence of the generated pseudo labels. Firstly, for each frame  $x_t$ , we generate a set of different class probabilities  $\mathbf{P}_t = \{\mathbf{p}_t^k\}_{k=1}^K$  by feeding  $x_t$  into the same network with random dropout  $K$  times, where  $\mathbf{p}_t^i \in \mathbb{R}^C$  and  $\mathbf{P}_t \in \mathbb{R}^{K \times C}$ . Then, we average these  $K$  vectors of probability, which can be formulated as  $\mu(\mathbf{P}_t) \in \mathbb{R}^C$ , where  $\mu(\cdot)$  is the mean function. After that, we obtain the class label for frame  $\mathbf{f}_t$  by:

$$c_t = \operatorname{argmax} \mu(\mathbf{P}_t). \quad (1)$$

Finally, we use the standard deviation to measure the uncertainty of the obtain class label, *i.e.*,  $u_t$ , which can be formulated as:

$$u_t = \sigma(\mathbf{P}_{t,c_t}), \quad (2)$$

where  $u_t$  is the uncertainty score.

After obtaining the uncertainty of each frame  $u_t$ , we use the temporal diffusion module to generate more pseudo labels for training in the next iteration; see the iterative training details in Sec. 3.3. Then, we treat the labeled frames as anchors and start pseudo-labeling from anchors to both sides in temporal dimension, which can be formulated as:

$$\tilde{y}_t = \begin{cases} y_t \cdot \mathbb{1}(u_t < \tau) \cdot \mathbb{1}(\tilde{y}_{t+1} = y_t), & t_{c-1} < t < t_c, \\ y_t \cdot \mathbb{1}(u_t < \tau) \cdot \mathbb{1}(\tilde{y}_{t-1} = y_t), & t_c < t < t_{c+1} \end{cases}, \quad (3)$$

---

**Algorithm 1** Loop training with Uncertainty-aware Temporal Diffusion

**Input:** Image set  $\mathbf{X} = \{x_t\}$ , timestamp label set  $Y_{ts} = \{y_t\}$ , initial CNN model  $f_0$ , initial TCN model  $g_0$ , uncertainty threshold  $\tau$ , forward times  $K$ , times of temporal diffusion  $n$ , times of loop training  $m$ .

**Output:** Well trained CNN model  $f$  and TCN model  $g$ .

```

1:  $\mathbf{Y} \leftarrow Y_{ts}$ 
2: for  $i = 1$  to  $n$  do
3:    $\triangleright$  Re-train model once acquiring newly labels
4:    $f \leftarrow \text{TrainCNN}(f_0, \mathbf{X}, \mathbf{Y}, \mathcal{L}_{ce})$ 
5:    $\mathbf{Y} \leftarrow \text{UATD}(f, \mathbf{X}, Y_{ts}, \tau, K)$             $\triangleright$  See Eq. 3
6: end for
7: for  $j = 1$  to  $m$  do
8:    $\mathbf{F} \leftarrow \text{ExtractFeatures}(f, \mathbf{X})$ 
9:   for  $i = 1$  to  $n$  do
10:     $g \leftarrow \text{TrainTCN}(g_0, \mathbf{F}, \mathbf{Y}, \mathcal{L}_{ce}, \mathcal{L}_{smooth})$ 
11:     $\mathbf{Y} \leftarrow \text{UATD}(g, \mathbf{F}, Y_{ts}, \tau, K)$ 
12: end for
13:    $\triangleright$  Transfer the labels TCN learns to CNN
14:    $f \leftarrow \text{TrainCNN}(f_0, \mathbf{X}, \mathbf{Y}, \mathcal{L}_{ce})$ 
15: end for

```

---

where  $\tau$  is the uncertainty threshold,  $t_c$  is the annotated timestamp and  $\tilde{y}_t$  is the diffused pseudo labels. In this way, the diffusion is stopped by high-uncertainty frames, *i.e.*, ambiguous ones.

### 3.3 Loop Training

As shown in Fig. 3 (c), we train our models in a loop manner. We first describe four main steps in our loop training: **(a)**  $f \leftarrow \text{TrainCNN}(f_0, \mathbf{X}, \mathbf{Y}, \mathcal{L}_{ce})$ , **(b)**  $\mathbf{F} \leftarrow \text{ExtractFeatures}(f, \mathbf{X})$ , **(c)**  $g \leftarrow \text{TrainTCN}(g_0, \mathbf{F}, \mathbf{Y}, \mathcal{L}_{ce}, \mathcal{L}_{smooth})$  and **(d)**  $\mathbf{Y} \leftarrow \text{UATD}(o, \mathbf{x}, y, \tau, K)$ .

**(a)**  $f \leftarrow \text{TrainCNN}(f, \mathbf{X}, \mathbf{Y}, \mathcal{L}_{ce})$ . Let we denote the frames of videos as  $\mathbf{X} = \{x_t\}_{t=1}^T$ , where  $T$  is the length of video. After feeding  $\mathbf{X} = \{x_t\}_{t=1}^T$  into the CNN  $f$ , we obtain its corresponding phase prediction  $\mathbf{p}_{t, \tilde{y}_t}^{cnn}$ . Then, the objective of the CNN, *i.e.*, **CrossEntropy Loss**, can be formulated as:

$$\mathcal{L}_{ce}(\mathbf{Y}, \mathbf{p}_t^{cnn}) = \frac{1}{T} \sum_{\tilde{y}_t \neq 0} -\log(\mathbf{p}_{t, \tilde{y}_t}^{cnn}), \quad (4)$$

where  $\mathbf{Y} = \{\tilde{y}_t\}_{t=1}^T$  is the target label.

**(b)**  $\mathbf{F} \leftarrow \text{ExtractFeatures}(f, \mathbf{X})$ . we use the trained  $f$  to extract spatial features of frame  $x_t$ , which is defined as  $\mathbf{F} = \{\mathbf{f}_t\}_{t=1}^T$ .

**(c)**  $g \leftarrow \text{TrainTCN}(g, \mathbf{F}, \mathbf{Y}, \mathcal{L}_{ce}, \mathcal{L}_{smooth})$ . After feeding  $\mathbf{F}$  into TCN  $g$ , we capture the temporal relations of frames in videos and obtain the final prediction  $\mathbf{p}_t^{tcn}$ .

We use the CrossEntropy loss to train the TCN, similar as CNN, *i.e.*,  $\mathcal{L}_{ce}(\mathbf{Y}, \mathbf{p}_t^{tcn})$ . Compared with the CNN, to encourage a smooth transition between frames, we use the truncated mean squared error as a **Smoothing Loss** following [10, 29]:

$$\mathcal{L}_{smooth} = \frac{1}{TC} \sum_{t,c} \tilde{\Delta}_{t,c}^2, \quad (5)$$

$$\tilde{\Delta}_{t,c}^2 = \begin{cases} \Delta_{t,c}^2, & \Delta_{t,c} < \gamma \\ \gamma, & otherwise \end{cases}, \quad (6)$$

$$\Delta_{t,c} = |\log(\mathbf{p}_{t,c}) - \log(\mathbf{p}_{t-1,c})| \quad (7)$$

where  $T$  is the video length,  $C$  is the number of action classes and  $\mathbf{p}_{t,c}$  is the probability of action  $c$  at time  $t$ . This loss function explicitly penalize the difference of each two adjacent frames and we suggest readers refer to [10] for more details. The final loss function is the weighted sum of these two losses:

$$\mathcal{L} = \mathcal{L}_{ce} + \lambda \mathcal{L}_{smooth}, \quad (8)$$

where  $\lambda$  is a hyper-parameter to balance the contribution of each loss and is set to 0.015 for all of our experiments.

**(d)**  $\mathbf{Y} \leftarrow \text{UATD}(o, \mathbf{x}, y, \tau, K)$ . Based on model  $o$ , video data  $x$ , corresponding labels  $y$ , uncertainty threshold  $\tau$  and forward times  $K$ , we can generate more pseudo labels by UATD, which is described in Sec. 3.2.

As illustrated in Alg. 1, we describe the details of training by the followings. First of all, we initialize the target label from timestamp supervision, *i.e.*,  $\mathbf{Y} \leftarrow Y_{ts}$ . Then we train CNN by performing modules **(a)**  $f \leftarrow \text{TrainCNN}(f, \mathbf{X}, \mathbf{Y}, \mathcal{L}_{ce})$  and **(d)**  $\mathbf{Y} \leftarrow \text{UATD}(f, \mathbf{X}, Y_{ts}, \tau, K)$  iteratively  $n$  times. Each iteration CNN is trained better by newly acquired labels and the diffusion will be wider next time. After obtaining a trained CNN  $f$ , we introduce an  $m$ -loops training. At the beginning of each loop, video feature is obtained by module **(b)**  $\mathbf{F} \leftarrow \text{ExtractFeatures}(f, \mathbf{X})$ . With video feature  $\mathbf{F}$ , we train TCN by performing modules **(c)**  $g \leftarrow \text{TrainTCN}(g_0, \mathbf{F}, \mathbf{Y}, \mathcal{L}_{ce}, \mathcal{L}_{smooth})$  and **(d)**  $\mathbf{Y} \leftarrow \text{UATD}(g, \mathbf{F}, Y_{ts}, \tau, K)$ . Since CNN lacks the ability of modeling temporal relationship, it can not generate sufficient pseudo labels. Therefore, we transfer the labels TCN generates to CNN in return at the end of each loop. In this way, CNN learns better representations by sufficient labeled data and then TCN generate more refined labels by meaningful features.

## 4 Experiments

### 4.1 Datasets and Metrics

**M2CAI16.** The M2CAI16 dataset [44] consists of 41 laparoscopic videos that are acquired at 25fps of cholecystectomy procedures, and each frame has a resolution of

Table 1: Comparison with the state-of-the-art on Cholec80 and M2CAI16 datasets.

Method	Cholec80				M2ca16			
	AC (%)	PR (%)	RE (%)	JA (%)	AC (%)	PR (%)	RE (%)	JA (%)
Fully Supervised Methods - 100% annotation time								
PhaseNet [45]	78.8 $\pm$ 4.7	71.3 $\pm$ 15.6	76.6 $\pm$ 16.6	-	79.5 $\pm$ 12.1	-	-	64.1 $\pm$ 10.3
EndoNet [46]	81.7 $\pm$ 4.2	-	79.6 $\pm$ 7.9	-	-	-	-	-
SV-RCNet [20]	85.3 $\pm$ 7.3	80.7 $\pm$ 7.0	83.5 $\pm$ 7.5	-	81.7 $\pm$ 8.1	81.0 $\pm$ 8.3	81.6 $\pm$ 7.2	65.4 $\pm$ 8.9
OHFM [50]	87.3 $\pm$ 5.7	-	-	67.0 $\pm$ 13.3	85.2 $\pm$ 7.5	-	-	68.8 $\pm$ 10.5
Casual TCN [29]	87.9 $\pm$ 8.2	86.4 $\pm$ 7.7	84.8 $\pm$ 12.9	72.4 $\pm$ 9.42	81.9 $\pm$ 11.3	84.8 $\pm$ 5.2	82.2 $\pm$ 9.0	68.1 $\pm$ 8.5
TeCNO [5]	88.6 $\pm$ 7.8	86.5 $\pm$ 7.0	88.8 $\pm$ 17.4	75.1 $\pm$ 6.9	-	-	-	-
TMRNet [22]	90.1 $\pm$ 7.6	90.3 $\pm$ 3.3	89.5 $\pm$ 5.0	79.1 $\pm$ 5.7	87.0 $\pm$ 8.6	87.8 $\pm$ 6.9	88.4 $\pm$ 5.3	75.1 $\pm$ 6.9
Trans-SVNet [13]	90.3 $\pm$ 7.1	90.7 $\pm$ 5.0	88.8 $\pm$ 7.4	79.3 $\pm$ 6.6	87.2 $\pm$ 9.3	88.0 $\pm$ 6.7	87.5 $\pm$ 5.5	74.7 $\pm$ 7.7
TCN [29]	91.1 $\pm$ 6.7	90.8 $\pm$ 4.5	87.6 $\pm$ 11.7	79.1 $\pm$ 8.5	82.9 $\pm$ 10.8	85.8 $\pm$ 5.4	82.7 $\pm$ 9.0	69.7 $\pm$ 8.7
Not end-to-end [51]	91.5 $\pm$ 7.1	-	87.2 $\pm$ 8.2	77.2 $\pm$ 11.2	88.2 $\pm$ 8.5	-	91.4 $\pm$ 11.2	75.1 $\pm$ 10.6
Semi Supervised Methods - 50% annotation time								
LRTD [39]	82.5 $\pm$ 8.4	79.7 $\pm$ 9.0	80.9 $\pm$ 8.1	64.2 $\pm$ 10.2	72.1 $\pm$ 13.7	74.1 $\pm$ 14.9	74.0 $\pm$ 10.4	54.4 $\pm$ 12.9
SurgSSL [40]	87.0 $\pm$ 7.4	84.2 $\pm$ 8.9	85.2 $\pm$ 11.1	70.5 $\pm$ 12.6	79.6 $\pm$ 9.4	80.2 $\pm$ 11.3	79.6 $\pm$ 11.5	62.0 $\pm$ 11.1
Timestamp Supervised Methods - 17% annotation time								
Casual TCN+Ours	88.6 $\pm$ 6.7	86.1 $\pm$ 6.7	88.0 $\pm$ 10.1	73.7 $\pm$ 10.2	86.0 $\pm$ 7.8	85.0 $\pm$ 6.2	87.1 $\pm$ 7.7	71.4 $\pm$ 10.4
TCN+Ours	91.9 $\pm$ 5.6	89.5 $\pm$ 4.4	90.5 $\pm$ 5.9	79.9 $\pm$ 8.5	87.6 $\pm$ 8.7	88.2 $\pm$ 7.4	87.9 $\pm$ 9.6	75.7 $\pm$ 9.5

1920  $\times$  1080. Following [51], 27 videos are used for training while the rest 14 are used for testing. These videos are segmented into 8 phases by experienced surgeons.

**Cholec80.** The cholec80 dataset [46] contains 80 videos of cholecystectomy surgeries performed by 13 surgeons. All the videos are recorded at 25 fps, and the frames in them have the resolution of 1920  $\times$  1080 or 854  $\times$  480. The dataset is divided into two subsets of equal size, with the first 40 videos as a training set and the other 40 as a testing set.

**Evaluation metrics.** Following previous works [20, 22, 46, 50], we utilize four metrics, *i.e.*, accuracy (AC), precision (PR), recall (RE), and Jaccard (JA), to evaluate the phase prediction accuracy. Among them, accuracy and Jaccard index are used to evaluate the submission of M2CAI Workflow Challenge, while precision and recall are also commonly used metrics for video-based phase recognition.

## 4.2 Implementation Details

Our code is based on PyTorch using an NVIDIA GeForce RTX 3090 GPU. We downsample the video to 1fps for training in all experiments following previous works [20, 22, 46]. All the frames are resized to a resolution of 250  $\times$  250, and data augmentations including 224  $\times$  224 cropping, random mirroring, and color jittering are applied during the training stage. We get a pre-trained inception-v3 [43] on ImageNet [23]. The batch size is set to 8, and an Adam optimizer with an initial learning rate of  $1e-4$  and weight decay of  $1e-5$  is used. We further use a step learning rate scheduler where the step size is two epochs and decay rate is 0.5 for fine-tuning by 5 epochs. To train TCN, we use Adam optimizer with an initial learning rate of  $1e-3$  and cosine annealing for learning rate decay. For all experiments, we set a dropout rate of 0.5 and an uncer-

tainty threshold  $\tau = 0.1$ ; the detailed analysis is shown in Table 4. The uncertainty is estimated by 5 forward times Monte Carlo Dropout. [12]. The numbers of rounds of uncertainty-aware temporal diffusion and loop training are set to 4 and 2, respectively. Furthermore, the timestamp annotations are simulated by randomly selecting one frame from each action phase in the training videos.

## 4.3 Comparison with the State-of-the-Arts

We compare our *less is more* method with the state-of-the-arts on the Cholec80 and M2CAI16 datasets, and report their results in Table 1. It is clear that our method outperforms previous data-efficient methods, *i.e.*, semi-supervised ones, on both data efficiency and phase recognition performance. For example, our timestamp supervision only requires 17% annotation time of the full supervision [32], while semi-supervision needs 50% annotation time [39]. Moreover, our method with the casual TCN [29] achieves 88.6% of accuracy on Cholec80 dataset, outperforms SurgSSL [40] over 1.6%. We can also find that our method can even achieve the competitive performance compared with the fully supervised methods, with only 17% annotation time of them. For example, our method with casual TCN is little inferior to TeCNO [5] which shares a similar backbone with us while it uses extra tool presence annotations. In addition, our method with TCN can outperform all existing method on Cholec80 dataset and achieve the second best on M2CAI16 dataset. Note that using the same backbone, our method outperforms fully supervised methods, as shown in the green and pink rows. Notably, the improvements of our method are more significant in M2CAI16 than in Cholec80. This is because M2CAI16 contains more ambiguous frames [6], which degrades the



Figure 4: Quality comparison to Li *et al.* [29]. In each sub-figure, the top is pseudo label by our method, the middle is the ground truth, and the bottom is pseudo label by Li *et al.* [29]. The top sub-figures are videos from Cholec80 while the bottom from M2CAI16.

Table 2: Comparison with different timestamp supervision methods.

Method	AC (%)	PR (%)	RE (%)	JA (%)
Cholec80				
Naive	66.92	62.28	74.81	48.23
Uniform	58.69	55.47	65.91	39.04
Li <i>et al.</i> [29]	79.37	78.67	85.41	63.99
Ours	<b>88.56</b>	<b>86.05</b>	<b>88.00</b>	<b>73.72</b>
M2CAI16				
Naive	67.48	58.73	61.70	44.80
Uniform	56.52	56.72	56.98	38.22
Li <i>et al.</i> [29]	72.70	76.47	80.48	59.96
Ours	<b>85.95</b>	<b>84.96</b>	<b>87.05</b>	<b>71.43</b>

performance. The details why our methods can outperform corresponding backbones in fully supervised setup will be discussed in Sec. 4.5.

#### 4.4 Comparison with Different Timestamp Supervision Methods

To evaluate the efficiency of our proposed uncertainty-aware temporal diffusion (UATD) for surgical video timestamp supervision, we compare our methods with two baseline models following [29], *i.e.*, Naive and Uniform, and report the results in Table 2. Specifically, Naive only computes the loss at the annotated timestamps while Uniform baseline generates the frame-wise labels by assuming that action labels change at the center frame between consecutive timestamps. It is clear that our method outperforms other two methods with a clear margin. Furthermore, we also compare Li *et al.* [29], which is the SOTA in action segmentation under this setting. It uses the middle output of model *i.e.*, features of frames to detect action change and generate frame-wise pseudo labels. However, using feature similarity to detect action change could be confused when the boundaries are generally ambiguous. As shown in Fig. 4, our methods give accurate pseudo labels by stopping dif-

fusion near boundaries while [29] attempts to give unappealing labels. From Table. 2, we can also see that our method obtains 7% – 13% improvements over all metrics.

Table 3: Ablative study of key components on Cholec80 dataset. ‘UATD<sup>1</sup>’ indicates using this method in the first stage *i.e.* CNN, while ‘UATD<sup>2</sup>’ means in the second stage *i.e.* TCN. ‘LP’ indicates the loop training which is defined in Sec. 3.3.

UATD <sup>1</sup>	UATD <sup>2</sup>	LP	AC (%)	PR (%)	RE (%)	JA (%)
✗	✗	✗	66.92	62.28	74.81	48.23
✓	✗	✗	82.28	78.05	86.87	65.96
✗	✓	✗	77.62	77.34	80.96	61.26
✓	✓	✗	85.59	83.54	86.60	70.85
✓	✓	✓	<b>88.56</b>	<b>86.05</b>	<b>88.00</b>	<b>73.72</b>

#### 4.5 Ablation Study

**Effect of UATD and LP.** There are two key components, *i.e.*, uncertainty-aware temporal diffusion (UATD) and loop training (LP), in our method. We ablate the effect of them in Table. 3. It is clear that the proposed UATD can improve the timestamp supervision with a clear margin, *e.g.*, combined with UATD, the model achieves 85.59% accuracy, outperforming 18.67% over the baseline model. Also, we could find that loop training contributes to around 3% improvements.

**Impact of the uncertainty threshold  $\tau$ .** the quality of pseudo labels is depended on pseudo labeling rate and pseudo labels accuracy, which is controlled by the uncertainty threshold  $\tau$  in Eq. 3. In order to evaluate the effect of  $\tau$ , we compare the performance of the models with different  $\tau$  and report the results in Table 4. We can find that the higher uncertainty threshold would lead to the higher pseudo labeling rate and the lower accuracy of pseudo labels, and vice versa. For example, with infinity threshold, *i.e.*, first row in Table 4, pseudo labeling rate can reach

Table 4: Quantitative results of different uncertainty threshold on M2CAI16.

	AC (%)	PR (%)	RE (%)	JA (%)	Labeling Rate (%)	Labeling Accuracy (%)
$\tau = \infty$	84.65	86.34	84.65	70.43	<b>93.49</b>	92.04
$\tau = 0.2$	85.32	<b>86.71</b>	85.06	71.14	92.72	94.13
$\tau = 0.1$	<b>85.95</b>	84.96	<b>87.05</b>	<b>71.43</b>	87.51	96.99
$\tau = 0.05$	85.49	86.19	86.42	71.20	60.76	<b>99.04</b>

Table 5: Change of labeling rate and labeling accuracy by Iteration of UATD on M2CAI16. TS indicates the initial timestamp annotations.

Iteration	TS	1st	2nd	3rd	4th
Labeling Rate (%)	0.33	67.70	76.82	84.45	87.51
Labeling Accuracy (%)	100.00	98.69	97.95	97.42	96.99

93.49% while accuracy of pseudo labels is only 92.04%. Such higher labeling rate would introduce more noisy labels, which degrades the labeling accuracy. In our paper, we set  $\tau$  to 0.1 for the best trade-off.

In addition, with the same threshold, as the diffusion goes pseudo labeling rate climbs up while accuracy of pseudo labels gets a fall; see Table. 5. This is because each iteration of temporal diffusion gives temporal model extra information, the model can generate more pseudo labels next time.

**Comparison of generated pseudo label and ground-truth.** In our experiments, we find that our method only generates pseudo labels for discriminative frames while ignores the ambiguous ones near boundaries. As shown in Fig. 5, our generated pseudo labels discard ambiguous or meaningless frames compared to the ground-truth. More importantly, the model trained with our generated pseudo labels outperforms the model trained with the ground-truth; see the green and pink rows of Table. 1. This is because ambiguous boundary of two adjacent actions is harmful for

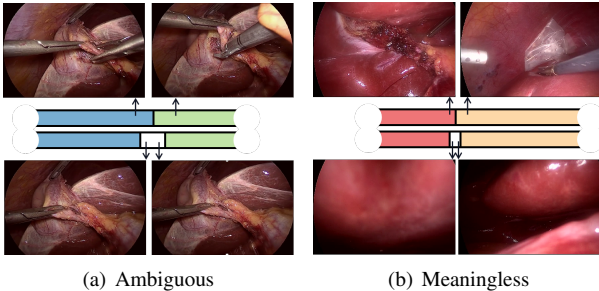


Figure 5: Quality comparison of generated pseudo labels and ground-truth. (a) Ambiguous frames in the action change from **CalotTriangleDissection** to **ClippingCutting**. (b) The moving of camera lead to some meaningless frames in the boundary between **CleaningCoagulation** and **GallbladderRetraction**.

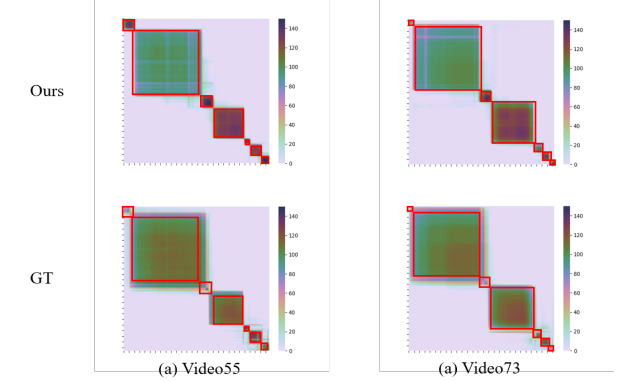


Figure 6: Correlation matrices on testset of Cholec80. The matrix is obtained from  $\mathbf{F} \times \mathbf{F}^T \in R^{T \times T}$ , where  $\mathbf{F} \in R^{T \times D}$  is a video feature. Deeper color represents high similarity between two frames. The **Red Box** indicates the ground truth phases of test video.

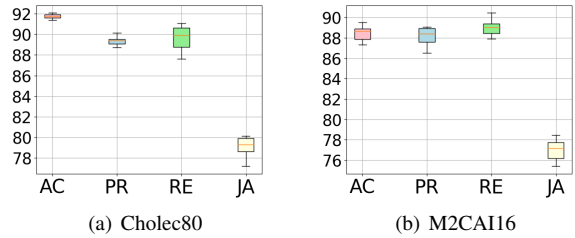


Figure 7: Box plots of random timestamp positions on Cholec80 and M2CAI16 datasets.

model to take apart from these two actions. To further explain this phenomenon, we visualize the correlation matrices of frame features, which are generated by the models trained with our generated pseudo labels and the ground-truth in Fig. 6. It is clear, when training the model with our labels, the features from different phases have more clear boundaries than the model with the ground-truth; see **Red Box** in Fig. 6.

**Effect of random timestamp positions.** In our experiments, the timestamp annotations are generated by randomly selecting one frames to be annotated of each phase. In order to evaluate the robust of our method to the different timestamp positions, we simulate 10 different random timestamp annotations by different random seeds and analyse theirs impacts to our method's performance. As shown in Fig 7, we report the box plots of 10 random positions on Cholec80 and M2CAI16 datasets. The short and flat boxes indicate that our proposed method is robust to different timestamp positions with a standard deviation less than 1% in all metrics. What's more, our method can outperform most of methods in Table. 1 with even the worst timestamp

Table 6: Quantitative results of Start, End, Middle and Random timestamp positions on Cholec80 dataset.

Timestamp Position	AC (%)	PR (%)	RE (%)	JA (%)
Start	90.64	87.92	88.37	76.75
End	90.17	88.35	82.24	70.75
Middle	<b>92.59</b>	<b>90.13</b>	<b>89.60</b>	<b>80.04</b>
Random	91.86	89.51	90.52	79.90

Table 7: Effectiveness of boundary mask on Cholec80 dataset.

Mask width	AC (%)	PR (%)	RE (%)	JA (%)
0	91.14	90.84	87.64	79.14
3	92.04	91.87	89.07	81.44
5	92.31	92.26	89.52	82.12
10	<b>92.75</b>	92.86	<b>90.57</b>	<b>83.32</b>
20	92.68	<b>93.20</b>	90.40	82.66

annotations. Furthermore, we explore the effect of three extreme cases of timestamp annotations *i.e.* the annotated frames are located at the start, the middle and the end of the phase. As shown in Table. 6, annotating at the start and end frames of each phase would degrade the performance with a clear margin. This is because that frames near boundaries are generally ambiguous, which can be hard to act as an anchor of temporal diffusion. In the contrast, the positions of middle and random are more discriminative to represent current phases and thus can generate more correct pseudo labels. Actually, the surgeons *,i.e.*, the annotators, tend to label the discriminative frames because they can easily recognize them when seeing through the whole video [32], which ensure timestamp annotations efficient and effective.

#### 4.6 Using Our Method with Ground-Truth

As analyzed in Fig. 5, we find that our method can only generate labels for discriminative frames, instead of ambiguous frames. Since we have known that phase boundaries are generally ambiguous and over-fitting in these noisy labels degrades the generalization ability of models, it comes up that if we discard the ground-truth of these ambiguous frames can improve the performance. To this end, as shown in Fig. 8 (a), we mask some ground-truth labels, especially near boundaries, based on our generated pseudo labels. Specifically, given by the ground-truth, we randomly select one frame in each phase as the annotated labels, while discarding labels of other frames, which simulates timestamp annotations. Then we perform our proposed uncertainty-aware temporal diffusion to generate incomplete pseudo labels, where those ambiguous frames near boundaries still remain unlabeled. In this way, we

Table 8: Effectiveness of using UATD with the ground-truth (GT) on Cholec80 dataset. ‘Timestamp’ is using our generated pseudo labels by UATD from timestamp annotations and ‘GT w/ UATD’ indicates the ground-truth labels masked by UATD; see Sec. 4.6 for details.

Backbone	Annotation	AC (%)	PR (%)	RE (%)	JA (%)
Casual TCN	GT	87.94	86.40	84.81	72.40
	Timestamp	88.56	86.05	88.00	73.72
	GT w/ UATD	<b>91.18</b>	<b>89.88</b>	<b>90.93</b>	<b>79.76</b>
TCN	GT	91.14	90.84	87.64	79.14
	Timestamp	91.86	89.51	90.52	79.90
	GT w/ UATD	<b>92.75</b>	<b>91.23</b>	<b>93.10</b>	<b>83.89</b>

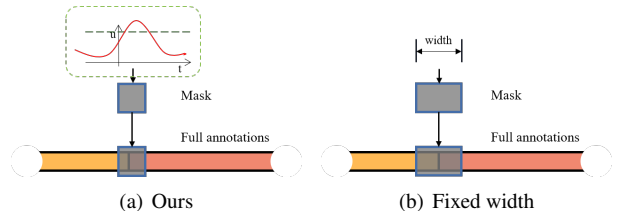


Figure 8: (a) Masking boundaries by using UATD to detect ambiguous frames. (b) Masking boundaries by fixed width.

use UATD to detect the ambiguous frames and discard them during training. We compare the performance of the models training with (a) GT, (b) pseudo labels generated by UATD and (a) GT masked by UATD, and report the results in Table 8. It is clear that the model training with GT masked by UATD can achieve the best results, even outperforms the current SOTA; see Table 1 for comparison. This indicates that our proposed UATD can mine the informative frames and clean the noisy labels, which boosts the generalization of the model. To prove this, we further conduct experiments on the models training with GT masked by the fixed width, which is similar to our method that not generating pseudo labels for the ambiguous boundaries, as shown in Fig. 8 (b). As illustrated in Table. 7, masking some frames near boundary during training outperform the model without masking over around 1% – 3% in all metrics. However, it will introduce a new hyper-parameter, *i.e.*, the width of mask, which is critical to the performance. Hence, in order to achieve the good performance, we need to conduct experiments to find the best choice, which is very time-consuming. *On the contrary, our method can be used as an approach to clean the noisy labels in the ground-truth automatically, without the need of hand-designed width.*

## 5 Discussion

Surgical phase recognition is one key component of computer-assisted surgery systems, which advances context-awareness in modern operating rooms. However, most existing works require frame-wise annotations which

are expensive, expertise-required and error-prone [9]. In contrast, we introduce timestamp supervision which only requires annotating one frame for each phase in a video to this context. To solve this setting, we propose **Uncertainty-Aware Temporal Diffusion (UATD)** to generate pseudo labels for those unlabeled frames. The motivation is that the generated pseudo labels should match ground-truth to a large extent by leveraging temporal relationships among frames while avoid noisy labeling ambiguous boundaries.

Our method outperforms most SOTAs with full supervision and all label-efficient methods by a clear margin. Based on this, we argue that **less is more** in this task with two aspects. Firstly, compared to full supervision, timestamp supervision which requires far more less annotation effort is able to provide enough temporal cues for performing surgical phase recognition. Secondly, using less but clean/discriminative pseudo labels is better than more but noisy/ambiguous ones to achieve good generalization ability.

Although our method achieves promising results, there are some limitations. First, the temporal property we consider is not overall yet. The diffusion in our method assumes that the workflow is smooth without dramatic change and hardly any ambiguous frame occurs in the internal of phase. But such assumption may be false for other datasets and in the future we will study more comprehensive temporal relationship to handle the intra-phase discontinuity. Moreover, the training process we propose is time-consuming containing several iterations of training model from scratch. And we will design more elegant training process to link up the optimal learning from different annotations, *i.e.*, different rounds of temporal diffusion in our methods.

Finally, we expect community to focus more on label-efficient surgical video analysis. The weakly setting of videos, such as transcripts [18] and timestamp supervision, deserve further attention and exploiting. And the related ideas can be further investigated in other medical image analysis problems in CT [14, 17, 26, 28], MRI [27, 48, 53].

## 6 Conclusion

In this paper, we introduce the most annotation-saving setting, namely timestamp supervision, for surgical phase recognition. With timestamp supervision, we propose a novel uncertainty-aware temporal diffusion (UATD) method to generate trustworthy pseudo labels according to the labeled frames. Our main idea is to generate pseudo labels by considering the relationship among video frames. Results on two datasets show that our method can outperform the fully supervised setup, which reveals an interesting phenomenon less is more in this task. Moreover, we also find that our method can be used as a labeling clean approach to remove the noisy labels near boundaries to im-

prove the generalization of the current surgical phase recognition. This paper provides some insights for label-efficient surgical phase recognition and hopefully inspire researchers to design label-efficient surgical video analysis algorithms.

## References

- [1] B. Bhatia, T. Oates, Y. Xiao, and P. Hu. Real-time identification of operating room state from video. In *AAAI*, volume 2, pages 1761–1766, 2007.
- [2] T. Blum, H. Feußner, and N. Navab. Modeling and segmentation of surgical workflow from laparoscopic video. In *International Conference on Medical Image Computing and Computer-Assisted Intervention*, pages 400–407. Springer, 2010.
- [3] P. Bojanowski, R. Lajugie, F. Bach, I. Laptev, J. Ponce, C. Schmid, and J. Sivic. Weakly supervised action labeling in videos under ordering constraints. In *European Conference on Computer Vision*, pages 628–643. Springer, 2014.
- [4] N. Bricon-Souf and C. R. Newman. Context awareness in health care: A review. *international journal of medical informatics*, 76(1):2–12, 2007.
- [5] T. Czempiel, M. Paschali, M. Keicher, W. Simson, H. Feußner, S. T. Kim, and N. Navab. Tecno: Surgical phase recognition with multi-stage temporal convolutional networks. In *International Conference on Medical Image Computing and Computer-Assisted Intervention*, pages 343–352. Springer, 2020.
- [6] X. Ding and X. Li. Exploiting segment-level semantics for online phase recognition from surgical videos. *arXiv preprint arXiv:2111.11044*, 2021.
- [7] X. Ding, N. Wang, X. Gao, J. Li, X. Wang, and T. Liu. Weakly supervised temporal action localization with segment-level labels. *arXiv preprint arXiv:2007.01598*, 2020.
- [8] X. Ding, N. Wang, X. Gao, J. Li, X. Wang, and T. Liu. Kfc: An efficient framework for semi-supervised temporal action localization. *IEEE Transactions on Image Processing*, 30:6869–6878, 2021.
- [9] R. DiPietro and G. D. Hager. Automated surgical activity recognition with one labeled sequence. In *International conference on medical image computing and computer-assisted intervention*, pages 458–466. Springer, 2019.
- [10] Y. A. Farha and J. Gall. Ms-tcn: Multi-stage temporal convolutional network for action segmentation. In *Proceedings of the IEEE/CVF Conference on Computer Vision and Pattern Recognition*, pages 3575–3584, 2019.
- [11] I. Funke, S. Bodenstedt, F. Oehme, F. von Bechtolsheim, J. Weitz, and S. Speidel. Using 3d convolutional neural networks to learn spatiotemporal features for automatic surgical gesture recognition in video. In *International Conference on Medical Image Computing and Computer-Assisted Intervention*, pages 467–475. Springer, 2019.

[12] Y. Gal and Z. Ghahramani. Dropout as a bayesian approximation: Representing model uncertainty in deep learning. In *international conference on machine learning*, pages 1050–1059. PMLR, 2016.

[13] X. Gao, Y. Jin, Y. Long, Q. Dou, and P.-A. Heng. Trans-svnet: Accurate phase recognition from surgical videos via hybrid embedding aggregation transformer. *arXiv preprint arXiv:2103.09712*, 2021.

[14] E. Gibson, F. Giganti, Y. Hu, E. Bonmati, S. Bandula, K. Gurusamy, B. Davidson, S. P. Pereira, M. J. Clarkson, and D. C. Barratt. Automatic multi-organ segmentation on abdominal ct with dense v-networks. *IEEE transactions on medical imaging*, 37(8):1822–1834, 2018.

[15] A. Graves. Practical variational inference for neural networks. *Advances in neural information processing systems*, 24, 2011.

[16] K. He, X. Zhang, S. Ren, and J. Sun. Deep residual learning for image recognition. In *Proceedings of the IEEE conference on computer vision and pattern recognition*, pages 770–778, 2016.

[17] T. Heimann, B. Van Ginneken, M. A. Styner, Y. Arzhaeva, V. Aurich, C. Bauer, A. Beck, C. Becker, R. Beichel, G. Bekes, et al. Comparison and evaluation of methods for liver segmentation from ct datasets. *IEEE transactions on medical imaging*, 28(8):1251–1265, 2009.

[18] D.-A. Huang, L. Fei-Fei, and J. C. Niebles. Connectionist temporal modeling for weakly supervised action labeling. In *European Conference on Computer Vision*, pages 137–153. Springer, 2016.

[19] A. Huault, D. Sarikaya, K. L. Mut, F. Despinoy, Y. Long, Q. Dou, C.-B. Chng, W. Lin, S. Kondo, L. Bravo-Sánchez, et al. Micro-surgical anastomose workflow recognition challenge report. *arXiv preprint arXiv:2103.13111*, 2021.

[20] Y. Jin, Q. Dou, H. Chen, L. Yu, J. Qin, C.-W. Fu, and P.-A. Heng. Sv-rcnet: workflow recognition from surgical videos using recurrent convolutional network. *IEEE transactions on medical imaging*, 37(5):1114–1126, 2017.

[21] Y. Jin, H. Li, Q. Dou, H. Chen, J. Qin, C.-W. Fu, and P.-A. Heng. Multi-task recurrent convolutional network with correlation loss for surgical video analysis. *Medical image analysis*, 59:101572, 2020.

[22] Y. Jin, Y. Long, C. Chen, Z. Zhao, Q. Dou, and P.-A. Heng. Temporal memory relation network for workflow recognition from surgical video. *IEEE Transactions on Medical Imaging*, 2021.

[23] A. Krizhevsky, I. Sutskever, and G. E. Hinton. Imagenet classification with deep convolutional neural networks. *Advances in neural information processing systems*, 25:1097–1105, 2012.

[24] F. Lalys, L. Riffaud, D. Bouget, and P. Jannin. A framework for the recognition of high-level surgical tasks from video images for cataract surgeries. *IEEE Transactions on Biomedical Engineering*, 59(4):966–976, 2011.

[25] J. Li, P. Lei, and S. Todorovic. Weakly supervised energy-based learning for action segmentation. In *Proceedings of the IEEE/CVF International Conference on Computer Vision*, pages 6243–6251, 2019.

[26] X. Li, H. Chen, X. Qi, Q. Dou, C.-W. Fu, and P.-A. Heng. H-denseunet: hybrid densely connected unet for liver and tumor segmentation from ct volumes. *IEEE transactions on medical imaging*, 37(12):2663–2674, 2018.

[27] X. Li, Q. Dou, H. Chen, C.-W. Fu, X. Qi, D. L. Belavý, G. Armbrecht, D. Felsenberg, G. Zheng, and P.-A. Heng. 3d multi-scale fcn with random modality voxel dropout learning for intervertebral disc localization and segmentation from multi-modality mr images. *Medical image analysis*, 45:41–54, 2018.

[28] X. Li, L. Yu, H. Chen, C.-W. Fu, L. Xing, and P.-A. Heng. Transformation-consistent self-ensembling model for semisupervised medical image segmentation. *IEEE Transactions on Neural Networks and Learning Systems*, 32(2):523–534, 2020.

[29] Z. Li, Y. Abu Farha, and J. Gall. Temporal action segmentation from timestamp supervision. In *Proceedings of the IEEE/CVF Conference on Computer Vision and Pattern Recognition*, pages 8365–8374, 2021.

[30] D. Liu, Q. Li, T. Jiang, Y. Wang, R. Miao, F. Shan, and Z. Li. Towards unified surgical skill assessment. In *Proceedings of the IEEE/CVF Conference on Computer Vision and Pattern Recognition*, pages 9522–9531, 2021.

[31] Z. Liu, Y. Lin, Y. Cao, H. Hu, Y. Wei, Z. Zhang, S. Lin, and B. Guo. Swin transformer: Hierarchical vision transformer using shifted windows. *arXiv preprint arXiv:2103.14030*, 2021.

[32] F. Ma, L. Zhu, Y. Yang, S. Zha, G. Kundu, M. Feiszli, and Z. Shou. Sf-net: Single-frame supervision for temporal action localization. In *European conference on computer vision*, pages 420–437. Springer, 2020.

[33] L. Maier-Hein, S. S. Vedula, S. Speidel, N. Navab, R. Kikinis, A. Park, M. Eisenmann, H. Feussner, G. Forestier, S. Giannarou, et al. Surgical data science for next-generation interventions. *Nature Biomedical Engineering*, 1(9):691–696, 2017.

[34] P. Mettes, J. C. Van Gemert, and C. G. Snoek. Spot on: Action localization from pointly-supervised proposals. In *European conference on computer vision*, pages 437–453. Springer, 2016.

[35] D. Moltisanti, S. Fidler, and D. Damen. Action recognition from single timestamp supervision in untrimmed videos. In *Proceedings of the IEEE/CVF Conference on Computer Vision and Pattern Recognition*, pages 9915–9924, 2019.

[36] P. Nguyen, T. Liu, G. Prasad, and B. Han. Weakly supervised action localization by sparse temporal pooling network. In *Proceedings of the IEEE Conference on Computer Vision and Pattern Recognition*, pages 6752–6761, 2018.

[37] S. Paul, S. Roy, and A. K. Roy-Chowdhury. W-talc: Weakly supervised temporal activity localization and classification.

In *Proceedings of the European Conference on Computer Vision (ECCV)*, pages 563–579, 2018.

[38] A. Richard, H. Kuehne, and J. Gall. Action sets: Weakly supervised action segmentation without ordering constraints. In *Proceedings of the IEEE conference on Computer Vision and Pattern Recognition*, pages 5987–5996, 2018.

[39] X. Shi, Y. Jin, Q. Dou, and P.-A. Heng. Lrtd: long-range temporal dependency based active learning for surgical workflow recognition. *International Journal of Computer Assisted Radiology and Surgery*, 15(9):1573–1584, 2020.

[40] X. Shi, Y. Jin, Q. Dou, and P.-A. Heng. Semi-supervised learning with progressive unlabeled data excavation for label-efficient surgical workflow recognition. *Medical Image Analysis*, 73:102158, 2021.

[41] K. Simonyan and A. Zisserman. Very deep convolutional networks for large-scale image recognition. *arXiv preprint arXiv:1409.1556*, 2014.

[42] K. K. Singh and Y. J. Lee. Hide-and-seek: Forcing a network to be meticulous for weakly-supervised object and action localization. In *2017 IEEE international conference on computer vision (ICCV)*, pages 3544–3553. IEEE, 2017.

[43] C. Szegedy, V. Vanhoucke, S. Ioffe, J. Shlens, and Z. Wojna. Rethinking the inception architecture for computer vision. In *Proceedings of the IEEE conference on computer vision and pattern recognition*, pages 2818–2826, 2016.

[44] A. Twinanda, S. Shehata, D. Mutter, J. Marescaux, M. De Mathelin, and N. Padoy. Miccai modeling and monitoring of computer assisted interventions challenge, 2016.

[45] A. P. Twinanda, D. Mutter, J. Marescaux, M. de Mathelin, and N. Padoy. Single-and multi-task architectures for surgical workflow challenge at m2cai 2016. *arXiv preprint arXiv:1610.08844*, 2016.

[46] A. P. Twinanda, S. Shehata, D. Mutter, J. Marescaux, M. De Mathelin, and N. Padoy. Endonet: a deep architecture for recognition tasks on laparoscopic videos. *IEEE transactions on medical imaging*, 36(1):86–97, 2016.

[47] L. Wang, Y. Xiong, D. Lin, and L. Van Gool. Untrimmednets for weakly supervised action recognition and detection. In *Proceedings of the IEEE conference on Computer Vision and Pattern Recognition*, pages 4325–4334, 2017.

[48] T. Wang, X. Xu, J. Xiong, Q. Jia, H. Yuan, M. Huang, J. Zhuang, and Y. Shi. Ica-unet: Ica inspired statistical unet for real-time 3d cardiac cine mri segmentation. In *International conference on medical image computing and computer-assisted intervention*, pages 447–457. Springer, 2020.

[49] G. Yenger, D. Mutter, J. Marescaux, and N. Padoy. Less is more: Surgical phase recognition with less annotations through self-supervised pre-training of cnn-lstm networks. *arXiv preprint arXiv:1805.08569*, 2018.

[50] F. Yi and T. Jiang. Hard frame detection and online mapping for surgical phase recognition. In *International Conference on Medical Image Computing and Computer-Assisted Intervention*, pages 449–457. Springer, 2019.

[51] F. Yi and T. Jiang. Not end-to-end: Explore multi-stage architecture for online surgical phase recognition. *arXiv preprint arXiv:2107.04810*, 2021.

[52] T. Yu, D. Mutter, J. Marescaux, and N. Padoy. Learning from a tiny dataset of manual annotations: a teacher/student approach for surgical phase recognition. *arXiv preprint arXiv:1812.00033*, 2018.

[53] Y. Yu, Y. Xie, T. Thamm, E. Gong, J. Ouyang, C. Huang, S. Christensen, M. P. Marks, M. G. Lansberg, G. W. Albers, et al. Use of deep learning to predict final ischemic stroke lesions from initial magnetic resonance imaging. *JAMA network open*, 3(3):e200772–e200772, 2020.

[54] B. Zhang, A. Ghanem, A. Simes, H. Choi, A. Yoo, and A. Min. Swnet: Surgical workflow recognition with deep convolutional network. In *Medical Imaging with Deep Learning*, 2021.